

# BEAM SIZE AND EMITTANCE MEASUREMENTS DURING THE ALBA BOOSTER RAMP

U. Iriso and G. Benedetti  
CELLS, Cerdanyola, Spain

## Abstract

The beam emittance in the ALBA Booster is damped from 50 to 10 nm\*rad during the energy acceleration from 110 MeV to 3 GeV. The synchrotron radiation monitor installed in a dipole magnet provides the transverse beam size evolution along the energy ramp, which is then used to calculate the emittance evolution during the Booster ramp. We present the experimental set-up and technique of this measurement, and discuss the agreement between the measured parameters and theoretical values.

## INTRODUCTION

The ALBA Booster accelerates the beam coming from the Linac in a ramp of 145 ms from (usually) 110 MeV to 3 GeV. The Synchrotron Radiation Monitor (SRM) uses the radiation produced when the electron beam goes through a dipole to control beam size and relative position in a non-destructive way, thereby providing useful information to monitor the Booster performance.

Table 1: Booster parameters. The Twiss parameters ( $\beta_x, \beta_y, \eta_x$ ) in this table are given at the dipole center.

Parameter	Injection	Extraction
energy, $E$ [GeV]	0.11	3.0
hor emit., $\epsilon_x$ [nm-rad]	50	10
dipole field, $B$ [T]	0.168	0.873
max. current, $I$ [mA]		4.0
bending radius, $\rho$ [m]		11.52
hor / ver beta, $\beta_x/\beta_y$ [m]	1.56 / 10.6	
dispersion, $\eta_x$ [m]		0.14

In this paper, we use the measurement of the transverse beam size to evaluate the emittance evolution along the energy ramp. This is inferred from the Twiss parameters and the energy spread, which is also calculated using a theoretical model. Furthermore, we also describe the SRM experimental set-up and the considerations taken to properly infer the beam size, including measurements of the turn-by-turn beam position oscillations. Table 1 shows the main parameters relevant for these studies.

Preliminary results of ALBA Booster emittance measurement along the ramp were previously presented at Refs. [1, 2]. More measurements have been repeated since then. The differences between the results and the modelled values are discussed.

## THEORETICAL MODEL

The evolution of the beam emittance and energy spread during the acceleration ramp is affected by the adiabatic

and radiation damping, and the effect of the quantum excitation given by the photon emission. This is described by the differential equation [3]:

$$\frac{dA}{dt} = -A \left( \frac{\dot{E}}{E} + \frac{2}{\tau} \right) + G, \quad (1)$$

where  $E$  refers to the beam energy,  $\tau$  is the damping time, and  $A$  stands for any of these parameters: horizontal and vertical emittance,  $\epsilon_x$  and  $\epsilon_y$ , or energy spread,  $(\sigma_E/E)^2$ . In case of  $\epsilon_y$ , the quantum excitation term  $G$  is absent and it is not damped to zero only because of the coupling. Intra-beam scattering effects are neglected since they decrease sharply by increasing the beam energy, and they are very low at the injection energy and currents below 4 mA.

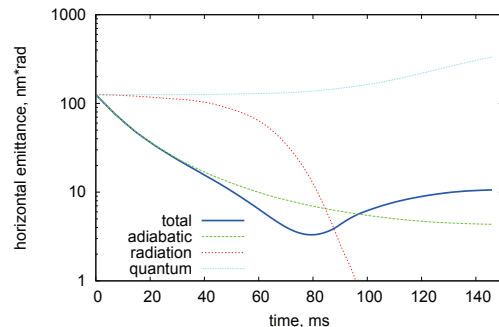


Figure 1: Evolution of each single term in Eq. 1, together with the total  $\epsilon_x$  (blue solid line) determined by the three terms acting together.

The three terms in Eq. 1 depend on the beam energy, which follows a  $\cos$  function with a cycle of 320 ms. Figure 1 shows the solution of  $\epsilon_x$  after numerically integrating Eq. 1. The emittance during the Booster ramp first decreases mainly due to the adiabatic damping, until after  $t \sim 80$  ms the quantum excitation makes the emittance increase slowly. This is shown by the solid blue line in Fig. 1, which also shows separately the emittance evolution due to the single effects of the adiabatic damping, radiation damping and quantum excitation.

## EXPERIMENTAL RESULTS

A sketch of the SRM is shown in Fig. 2. The SRM disposes of a slit to limit both the Depth Of Field (DOF) and the amount of light (to avoid CCD pixel saturation at high energy). A commercial telephoto lens whose focal lens is manually controlled allows us to zoom-in up to a Field Of View (FOV) of  $24.6 \times 18.7$  mm. The image is captured by a GigaBit Ethernet CCD (Basler Scout 1030gm) with a calibration of  $24.5 \mu\text{m}/\text{pixel}$ .

05 Beam Dynamics and Electromagnetic Fields

D01 Beam Optics - Lattices, Correction Schemes, Transport

The system is calibrated in the lab, and then installed in the Booster as a whole to keep the optical calibration of the system. Since high energy beam images are saturated, we install a light attenuator (Neutral Density filter OD1) to avoid the CCD saturation. This obliges us to increase the CCD exposure time for low energy images.

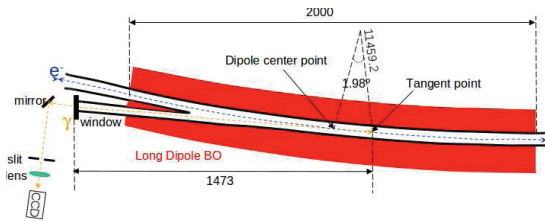


Figure 2: Sketch of the SRM.

### Beam size evolution

The evolution of the beam size along the Booster ramp is monitored as follows: we fix the CCD trigger at a certain time  $t$  in the ramp and take several beam pictures, between 4 and 10, for several beam injections. The images are analyzed on-line performing Gaussian fits to the horizontal and vertical projections. The beam size is taken as the average fit sigma for all the pictures, and the rms variation of the different fits at a given time is taken as the result error bar. We next move the trigger to another time, and repeat the sequence.

Imaging with SRM is affected by curvature error and diffraction limit. These terms add in quadrature to provide the system Point Spread Function (PSF), which corresponds to the image produced by a zero emittance beam. This is evaluated as [4, 5]

$$PSF^2 = (\rho\theta^2)^2 + (0.42\lambda/\theta)^2, \quad (2)$$

where the first term in Eq. 2 corresponds to the curvature error and the second is the Fraunhofer diffraction limit. The parameter  $\rho$  is the bending radius and  $\theta = 1.7$  mrad is the acceptance angle given by the slit. In our case, the  $PSF=140 \mu m$ , which is especially significant at high energies.

Figure 3 shows the comparison between modelled and measured beam sizes, where the beam size calculation already considers the PSF effect. In order to compute the modelled beam size, the emittance at injection is calculated from the beam size measurement at  $t = 0$ . After that, the model beam size is computed from the evolution of the  $\epsilon$  and the theoretical Twiss parameters. We can see that both measured and model beam sizes follow a similar evolution. Between  $t = [0-80]$  ms, the beam size in both vertical and horizontal plane are slightly larger, while for  $t > 80$  ms, the agreement is almost perfect.

In order to evaluate possible reasons for the differences seen for  $t < 80$  ms, we look at the turn-by-turn position oscillations measured by the BPMs.

### 05 Beam Dynamics and Electromagnetic Fields

#### D01 Beam Optics - Lattices, Correction Schemes, Transport

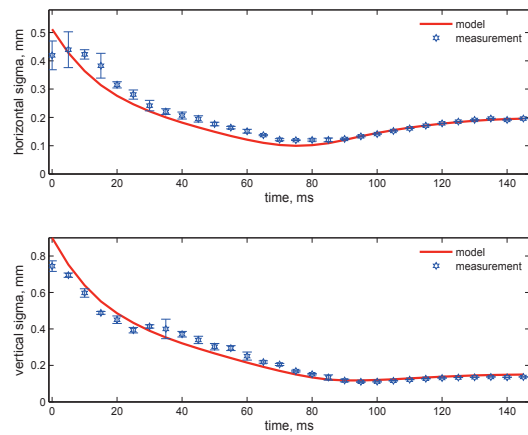


Figure 3: Results of the horizontal and vertical beam sizes along the Booster ramp. The measurements (blue stars) are compared with the model values (red solid lines).

### Turn by Turn Beam Position Oscillations

The apparent beam size measured by the SRM can be enlarged if the centroid position significantly moves during the CCD exposure time, especially at injection, when the exposure time is in the order of ms. The effect of the beam position oscillations can be neglected if the oscillations are much smaller than the beam size (which can be the case in Storage Rings, where the orbit is corrected below the  $1 \mu m$ ). But during the ALBA Booster ramp this approximation may not hold.

Figure 4 shows the rms position oscillation with respect to the closed orbit at the SRM source point during the energy ramp. The rms oscillations are estimated from the turn by turn data at a BPM located downstream the dipole holding the SRM and scaling them according to the  $\beta$  functions at both the BPM and SRM. We can see that the rms position oscillations are important just at injection (around  $\pm 0.3$  mm in both planes), and they reduce later to values in the order of single turn electronics resolution (around  $70 \mu m$  [6]). In Fig. 4, the oscillations for  $t > 10$  ms are seen slightly larger in the vertical plane due to the largest ratio in the  $\beta$  functions. Beam orbit oscillations are not the cause of the different beam sizes measured below 80 ms in Fig. 3.

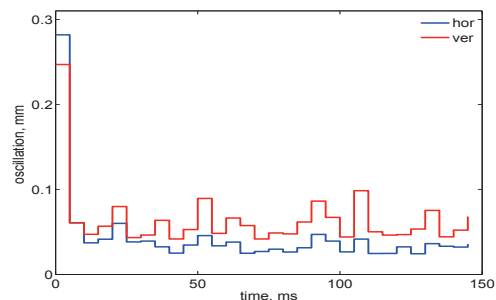


Figure 4: Measured hor and ver rms centroid oscillation around the orbit at the dipole center.

## COMPARISON BETWEEN MODELLED AND MEASURED EMITTANCES

The hor and ver emittances are calculated from the measured beam sizes  $\sigma_x$  and  $\sigma_y$  according to:

$$\sigma_x^2 = \beta_x \epsilon_x + \left( \eta_x \frac{\sigma_E}{E} \right)^2 \quad ; \quad \sigma_y^2 = \beta_y \epsilon_y \quad (3)$$

where the used values of beta functions, and dispersion are the theoretical ones. The initial value of  $\sigma_E/E$  is taken as the one measured at the Linac, and its evolution is computed from the numerical integration of Eq. 1. Proper energy matching is ensured by scanning the Booster rf phase and checking the horizontal beam size at injection (see Fig. 5), where we can see the large influence of the rf phase in the beam size.

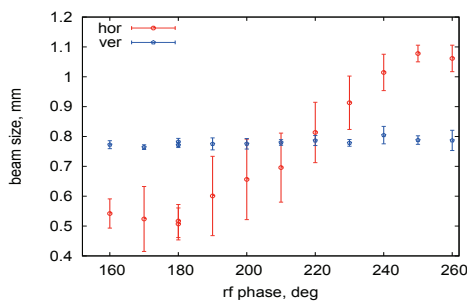


Figure 5: The hor beam size is minimized by varying the Booster rf phase, indicating a proper match between Linac and Booster.

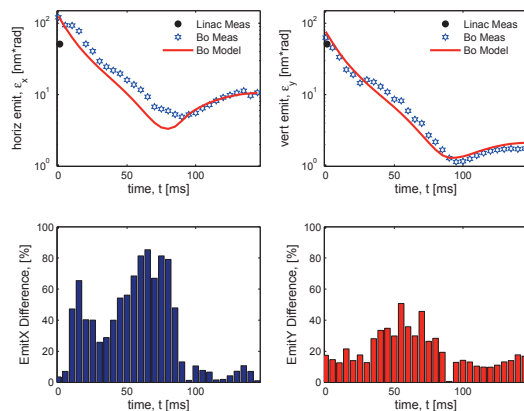


Figure 6: **Top:** comparison between emittance measurements (blue stars) and theoretical values (red lines). A coupling of 10% has been assumed for  $\epsilon_y$ . The black dots represent the Linac  $\epsilon$  measurement. **Bottom:** difference between model and measurement values of top plots.

Figure 6 (top) compares the measured and theoretical  $\epsilon_x$ ,  $\epsilon_y$ , while the bottom plots quantitative shows the comparison agreement. The emittances obtained by integrating Eq. 1 with starting values equal to the ones measured at injection time are fully satisfactory in the vertical plane

(within a  $\sim 15\%$ , which is below the  $\sim 25\%$  of possible error bars in the  $\beta$ -beating). In the hor plane the disagreement between [20-80] ms is more pronounced (on average  $\sim 60\%$ , see Fig. 6 - bottom), while an excellent agreement is found for  $t > 80$  ms, when the  $\epsilon_x$  is given by the equilibrium between dampint and quantum excitation. This is similar to what is observed with the beam sizes in Fig. 3.

There is a difference between the Linac  $\epsilon_x$  (black dot in Fig. 6 - top) and Booster measurement at injection. Together with the differences observed in the horizontal plane between [20-80]ms, this indicates that other non-modelled effects may occur, like a distortion of the beam energy distribution (due to jitters in the Linac energy and/or Booster dipole power supply), or filamentation due to a non-perfect matching between Linac and Booster. These cases would mainly affect the dispersive term in Eq. 3 and need further investigations. The tune variation along the first  $\sim 30$  ms is in the order of 0.1 units [1], which may also affects the emittance evolution through the coupling.

## CONCLUSIONS

A measurement of the horizontal and vertical Booster emittance evolution along the ramp has been performed using the SRM installed in one dipole. The overall comparison is satisfactory. We found a good agreement in the ver plane, but in the hor plane there are some discrepancies between [20-80]ms that need further investigations. These include simulations to check possible filamentation, use beam collimators in the transfer line to limit the effects of the Linac energy jitter, and extracting the beam at different energies and measuring the beam size at the transfer line.

## ACKNOWLEDGMENTS

J. Marcos is very appreciated for his help in the numerical integration of Eq. 1 with dedicated (*Mathematica*) scripts. We thank the Operations Group for their work and support in the Control Room.

## REFERENCES

- [1] G. Benedetti et al, *Modeling results of the ALBA Booster*, Proc. of IPAC'11 (2011).
- [2] M. Pont et al, *Operation of the ALBA Booster*, Proc. of IPAC'11 (2011).
- [3] M. Sands, *The Physics of Electron Storage Rings, An Introduction*. SLAC-121 (1970, addendum 1979).
- [4] A. Hofman and F. Meot, *Optical resolution of beam cross-section measurements by means of Synchrotron Radiation*, NIM 203 (1982) 483-493.
- [5] J.W. Flanagan, *Diagnostics for ultra-low emittance beams*, Proc. of IPAC'11, (2011).
- [6] U. Iriso, B. Benedetti, A. Olmos. *Beam Diagnostics at ALBA Linac*, Proc. of DIPAC'09 (2009).